

Magnetic and structural phase transitions in BaMnF₄

D. E. Cox, S. M. Shapiro, and R. A. Cowley*
Brookhaven National Laboratory, Upton, New York 11973

M. Eibschütz and H. J. Guggenheim
Bell Laboratories, Murray Hill, New Jersey 07974
 (Received 12 July 1978)

Elastic and inelastic neutron scattering experiments were performed on single and polycrystalline samples of BaMnF₄. The system orders magnetically below $T_N \approx 26$ K and the magnetic structure is shown to be similar to other members of the BaMF₄ family with $M = \text{Fe}$ and Ni, i.e., an antiferromagnetic ordering along both the b and c directions with a two-dimensional magnetic character perpendicular to b . The antiferromagnetic axis is rotated $\sim 9^\circ$ from the orthorhombic b axis and the ordered Mn²⁺ moment is $4.8\mu_B$. The spin-wave dispersion curves were measured and the exchange constants and anisotropy determined. The structural phase transition occurring at $T_c = 247$ K was studied in detail and shown to be incommensurate, with superlattice peaks below T_c at $\vec{q}_1 = (0.392, 0.5, 0.5)$ and multiples of this: $\vec{q}_2 = 2\vec{q}_1$ and $\vec{q}_3 = 3\vec{q}_1$. These wave vectors do not change with temperature. The phase transition appeared to be continuous with $\beta = 0.31 \pm 0.05$. The dynamical studies of this transition show a soft mode which becomes overdamped at \vec{q}_1 but becomes underdamped as \vec{q} increases away from \vec{q}_1 and as $T - T_c$ increases. High-resolution studies also show the existence of a diverging central peak. A theoretical description of the phase transition suggests the existence of four modes below T_c , corresponding to fluctuations of the amplitude and phase of the order parameter. We have as yet been unable to detect these different modes.

I. INTRODUCTION

BaMnF₄ is a member of a group of isostructural compounds which have unusual magnetic and electrical properties and have been the subject of numerous investigations in the past decade. Interest in these materials was stimulated by the discovery of both antiferromagnetism and piezoelectricity in crystals of BaMF₄ ($M = \text{Mn}, \text{Fe}, \text{Co}, \text{and Ni}$) in 1968 by Eibschütz and Guggenheim.¹ This was followed by the observation of ferroelectricity in the Mg, Co, Ni, and Zn compounds.² A spontaneous polarization could not be measured in BaMnF₄ and BaFeF₄ because of high electrical conductivity, but subsequent dielectric measurements³ showed a Curie-Weiss behavior for all six compounds with Curie temperatures above the respective melting points.

BaMnF₄ was first synthesized by Cousseins and Samouël.⁴ The crystal structure was determined in detail by Keve *et al.*⁵ shortly after von Schnering and Bleckmann had reported the results of a study of isostructural BaZnF₄.⁶

The room-temperature structure is orthorhombic, space group $A2_1am$ ($a = 5.9845 \text{ \AA}$, $b = 15.098 \text{ \AA}$, $c = 4.2216 \text{ \AA}$ at 298 K),⁵ and consists of MnF₆ octahedra linked at the corners to form puckered sheets

perpendicular to the b axis and separated by layers of Ba ions (Fig. 1). As pointed out by Brandon and Megaw,⁷ the structure can also be visualized as being composed of diagonal slabs of a perovskite-type lattice. Keve *et al.* also proposed a plausible model to account for the failure to observe polarization reversal in BaMnF₄, in contrast to BaZnF₄, on the basis of the differing interatomic distances involving Mn or Zn ions in the puckered sheets.

In common with the other magnetic compounds of this type, the magnetic properties of BaMnF₄ were found to show two-dimensional behavior,⁸ with a broad peak at about 50 K, and an antiferromagnetic transition at about 25 K. In addition, the observation of low-frequency magnetoelectric resonances was interpreted in terms of a two-dimensional model.⁹ It is therefore reasonable to expect the magnetic structure to be similar to those of BaNiF₄,¹⁰ and BaFeF₄.¹¹

Up to this point, there was no indication that BaMnF₄ was basically different from the other magnetic BaMF₄ compounds. However, measurements of the frequency and temperature dependence of the microwave elastic properties by Spencer *et al.*¹² showed a sharp anomaly in the elastic attenuation at about 255 K which they interpreted as indicative of a structural transition. Further evidence of a lowering

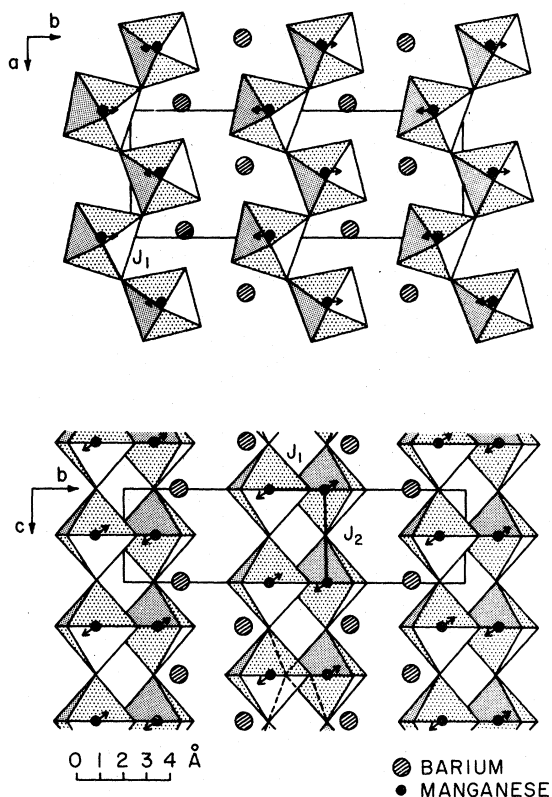


FIG. 1. Crystal structure of BaMnF₄ (after Keve *et al.*⁵) showing MnF₆ octahedra projected on (001) at top and (100) at bottom. Small arrows illustrate antiparallel coupling of Mn moments within puckered sheets as described in Sec. II. J_1 and J_2 are exchange interactions as discussed in Sec. III B.

of the symmetry was provided by the observation of a splitting of the lines in the ¹⁹F NMR spectrum¹³ and a small spontaneous magnetic moment below T_N .¹⁴ The latter suggests that the antiferromagnetic sublattices are not strictly collinear, a possibility also noted in the earlier work.⁸

Although Petrov *et al.*¹⁵ ruled out the presence of weak ferromagnetism on the basis of their antiferromagnetic resonance (AFMR) measurements, a subsequent study by Venturini and Morgenthaler¹⁶ revealed a splitting of one mode consistent with the presence of a weak Dzyaloshinsky-Moriya moment at 4.2 K along the c axis. They suggested that this canting might be masked in static magnetization measurements by the presence of domains with oppositely directed weak moments. In a recent paper, Fox and Scott have proposed that the weak ferromagnetism is induced by the spontaneous electric polarization via a linear magnetoelectric interaction.¹⁷

The existence of a structural phase transition at 255 K was confirmed in a Raman study.¹⁸ It was concluded that the transition was essentially continu-

ous and involved a doubling of the primitive unit cell, and was characterized by a soft optical phonon at the zone boundary of the orthorhombic phase. Additional Raman data have been reported by Popkov *et al.*¹⁹

A mechanism for the transition was proposed by Fritz on the basis of ultrasonic velocity and attenuation measurements.²⁰ This involves the rotation of MnF₆ octahedra about the b axis, the resulting symmetry being monoclinic, space group $P2_1$. It was further reported that although x-ray experiments had been unsuccessful in detecting a structural transition, the ionic displacements involved might be too small to be seen in this way. Recent Brillouin scattering measurements²¹ give sound velocities in agreement with the ultrasonic values above the transition temperature, but reveal that the wave-vector dependence of the transverse-acoustic phonons is anomalously dispersive.

Dielectric anomalies have been observed by Samara and Richards²² near to the structural transition, the most striking feature being a λ -shaped anomaly at 250 K in the static dielectric constant along the a axis, as predicted.¹⁸ However, similar measurements by Levstik *et al.*²³ did not show the predicted divergence. Another interesting feature of the Samara and Richards data is a maximum in the transition temperature as a function of pressure at about 10 kbar. Dielectric anomalies were also seen at about 70 and 30 K, and attributed to the onset of magnetic ordering.²⁴

Dvorak²⁵ has recently published a detailed group-theoretical analysis of the structural phase transition based upon a knowledge of the magnetic structures and magnetoelectric effects in the magnetic BaMF₄ compounds. Some of the characteristics of the transition are discussed, including possible symmetry changes and anomalies in the dielectric and elastic constants.

The present paper describes a neutron diffraction study of BaMnF₄ which has extended over a considerable period of time.²⁶ The original objective of this study was to determine the magnetic structure and some of the critical magnetic properties. The early powder diffraction data taken at 290 and 30 K gave very little indication of any structural change, but after the confirmation of the structural phase transition,¹⁸ an exhaustive search led to the discovery of a phase below 250 K with an incommensurate structure. Since then, considerable effort on single crystals has been devoted to a study of the critical and inelastic neutron scattering over a wide temperature range, particularly in the vicinity of both the magnetic and structural transitions, although the crystal structure of the low-temperature incommensurate phase has not yet been solved.

The paper is organized as follows. The results of the magnetic structure determination and the critical

magnetic experiments are described in Sec. II, and the magnetic excitations are described in Sec. III. In the analysis of these results, the incommensurate modulation of the basic structure has not been taken into account. The critical and inelastic scattering studies of the structural transition are described in Sec. IV. A theoretical analysis of the incommensurate transition is presented in Sec. V.

II. MAGNETIC STRUCTURE

A. Powder neutron data

Powder neutron scans were initially carried out at 290, 30, and 4.7 K with neutrons of wavelength 2.36 Å from a graphite monochromator. A pyrolytic graphite filter was used to suppress higher-order wavelengths. At 290 K, all the peaks can be indexed in terms of the orthorhombic cell [Fig. 2(a)] and analysis was carried out by the profile refinement technique.^{27,28} In view of the limited amount of data, no attempt was made to refine the atomic positional parameters or temperature factors, and these were assigned the values obtained by Keve *et al.*⁵ The refined values of the lattice parameters are listed in

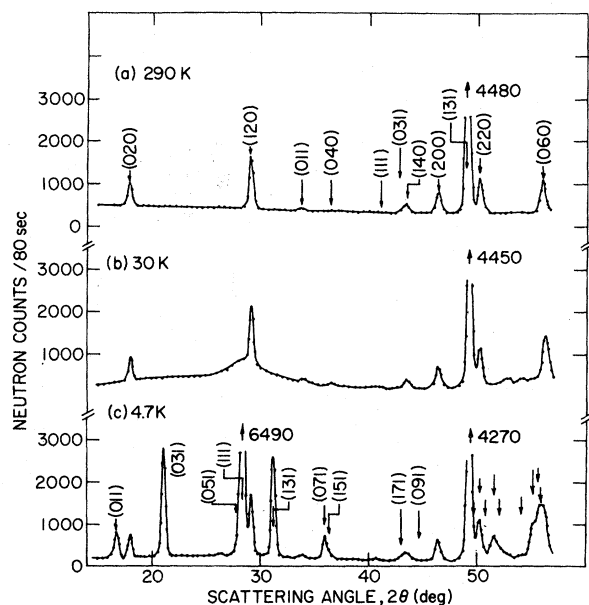


FIG. 2. Some of the powder neutron data from BaMnF_4 at various temperatures. (a) 290 K. Nuclear peaks are indexed. (b) 30 K. Note the strong magnetic diffuse scattering around 29° , and the two weak additional peaks around 53° . (c) 4.7 K. Arrows show magnetic peaks indexed in terms of an orthorhombic cell with b and c doubled.

Table I, together with the three R factors R_I , R_P , and R_{WP} which correspond to integrated intensities derived by the approximation described by Rietveld,²⁷ unweighted intensity data points, and weighted data points, respectively. Observed and calculated integrated intensities are compared in Table II, and agreement is seen to be quite satisfactory.

At 4.7 K, the pattern is characterized by the appearance of a number of additional peaks which can be indexed on the basis of a cell doubled along the b and c directions, with reflection conditions k and l both odd (or half integer with respect to the chemical cell) [Fig. 2(c)]. The intensity of one of the strong peaks of this type ($0\frac{3}{2}\frac{1}{2}$) was followed as a function of temperature and seen to vanish at about 26.5 K (Fig. 3). This corresponds closely to the anomaly in the perpendicular magnetic susceptibility previously noted.⁸

Thus the powder diffraction patterns of BaMnF_4 closely resemble those of BaNiF_4 ,⁹ and BaFeF_4 .¹⁰ Profile refinement of the 4.7 K data was carried out based upon the same type of magnetic structure, with the moment directed along the b axis. Once again, the atomic positional parameters were assigned the room-temperature values⁵ but the temperature factors were set equal to zero.²⁹ A good overall agreement was obtained ($R_{WP} = 16.5\%$), but some systematic discrepancies between some of the observed and calculated magnetic intensities were evident (Table III, Model 1). A much better fit was obtained by allowing the antiferromagnetic axis to rotate in the bc plane, (Table III, Model 2) as reflected in a significantly lower value for R_{WP} of 14.3%. A rotation of

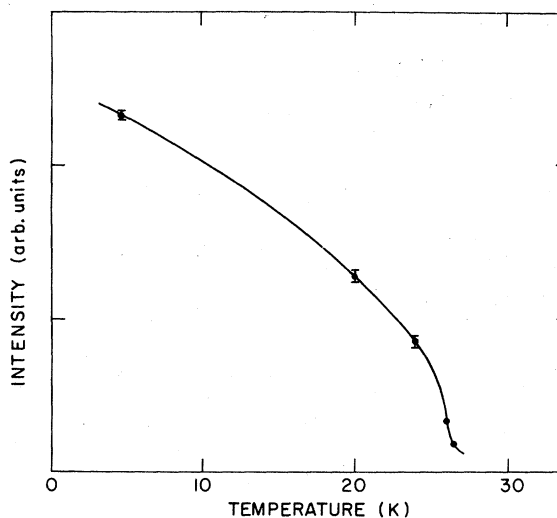


FIG. 3. Temperature dependence of integrated intensity of the $(0\frac{3}{2}\frac{1}{2})$ peak from BaMnF_4 powder.

TABLE I. Refined values of profile parameters for polycrystalline BaMnF₄. Ionic positional parameters and temperature factors as in Ref. 5. B is an extra negative overall temperature factor to allow for decreases in the latter as the temperature is lowered. Standard errors are given in parentheses and refer to the least significant digit.

	290 K	260 K	245 K	80 K	4.7 K ^a
a (Å)	5.998(1)	5.997(1)	5.999(1)	5.998(2)	5.994(1)
b (Å)	15.107(2)	15.101(3)	15.097(3)	15.055(5)	15.045(3)
c (Å)	4.221(1)	4.221(1)	4.217(1)	4.199(1)	4.194(1)
B (Å ²)	...	-0.5(4)	-0.6(4)	-1.2(6)	...
R_I (%)	9.3	8.7	8.4	9.5	9.6
R_P (%)	11.1	10.2	10.0	10.8	11.6
R_{WP} (%)	11.7	10.6	10.4	11.2	14.3

^aIncludes magnetic peaks. Magnetic structure as described in text, with temperature factors set equal to zero. $S_b = 4.73(5)\mu_B$ and $S_c = -0.75(7)\mu_B$.

this sort is permitted under the magnetic symmetry $P_{2a}2_1$ previously assigned for BaNiF₄.⁹ However, the inclusion of an a axis component of moment with appropriate symmetry, an overall temperature factor, or the Mn positional parameter as variables did not result in any further improvements. Final values of the profile parameters are listed in Table I. The nu-

clear intensities are given in Table II for easy comparison with the 290 K data. As mentioned earlier, the incommensurate modulation has not been taken into account in the above analysis. However, for reasons to be outlined in Sec. IV A, it is likely that this will have a negligible effect on the magnetic intensities.

The basic magnetic structure of BaMnF₄ at 4.7 K is

TABLE II. Comparison of observed and calculated nuclear intensities from polycrystalline BaMnF₄ at 290 and 4.7 K. Parameters as in Ref. 5 and Table I. Scattering lengths taken as 0.512×10^{-12} , -0.376×10^{-12} , and 0.565×10^{-12} cm for Ba, Mn, and F respectively.

hkl	290 K		4.7 K	
	I_{calc}	I_{obs}	I_{calc}	I_{obs}
0 2 0	28	26	25	26
1 2 0	56	60	51	74
0 1 1	3	2	2	3
0 4 0	1	1	2	2
1 1 1	0	0	0	2
0 3 1	2	0	1	1
1 4 0	10	11	14	12
2 0 0	22	26	23	31
1 3 1	243	231	253	247
2 2 0	41	47	51	53
0 6 0	53	50	50	66
0 5 1	201	188	221	201
2 1 1	382	412	432	466
1 5 1	288	250	335	276
2 3 1	259	296	297	350
0 0 2	142	155	166	166

TABLE III. Comparison of observed and calculated intensities of the first few magnetic peaks from polycrystalline BaMnF_4 at 4.7 K for the domain orientation chosen in Fig. 4. The observed intensities are obtained by the approximation described by Rietveld (Ref. 27), and may vary slightly depending upon the particular variables refined. Parameters as in Table I. Form factors for Mn^{2+} taken from Ref. 30.

	Model 1		Model 2	
	I_{calc}	I_{obs}	I_{calc}	I_{obs}
$0 \frac{1}{2} \frac{1}{2}$	34	30	31	30
$0 \frac{3}{2} \frac{1}{2}$	98	121	124	121
$0 \frac{5}{2} \frac{1}{2}$	55	41	33	31
$1 \frac{1}{2} \frac{1}{2}$	303	295	297	304
$1 \frac{3}{2} \frac{1}{2}$	106	118	117	118
$0 \frac{7}{2} \frac{1}{2}$	18	25	31	26
$1 \frac{5}{2} \frac{1}{2}$	7	7	6	6

depicted in Fig. 4. The antiferromagnetic axis is rotated about 9° from the orthorhombic b axis towards the doubled axis of the monoclinic cell, and the Mn^{2+} moment is $4.79\mu_B$. The corresponding magnetic symmetry is $P_{2a}2_1$ and there are two structurally equivalent domains as previously noted. This space group, of course, permits neither a ferromagnetic component, nor a magnetoelectric effect. However, if the crystal symmetry above T_N is assumed to be monoclinic $P2_1$, with the doubled unit cell shown in Fig. 4, the magnetic symmetry would be $P2_1'$. A fer-

romagnetic component perpendicular to the antiferromagnetic axis (i.e., roughly along the orthorhombic c axis) is now permitted, in agreement with published results,¹⁶ and the moment is qualitatively the right magnitude to be induced by the spontaneous electric polarization via a linear magnetoelectric effect.¹⁷ However, it is far too small to be detected in a diffraction experiment with unpolarized neutrons.

The diffraction data taken at 30 K show a very pronounced hump at low angles characteristic of long-range two-dimensional magnetic correlations [Fig. 2 (b)], but otherwise differ very little from the 290 K data. The only indication of an intermediate structural transformation is the presence of two very weak peaks at about 52.8 and 54.2° , respectively. However, these could not be indexed in terms of the chemical cell nor any simple multiple cell. Furthermore, the pattern in this region is complicated by the presence of some diffuse magnetic scattering, and at the time these experiments were performed no further attention was given to these two peaks. As we shall see later, these peaks correspond to superlattice peaks of the incommensurate phase.

B. Single-crystal data

The first crystal to be studied was cut from a piece of zone-melted material to dimensions of roughly $6 \times 2 \times 2 \text{ mm}^3$ in the a , b , and c directions, respectively. The crystal was mounted with the a axis vertical. Data taken at 77 and 4.5 K confirmed the magnetic structure determined from the powder data. Because of rather severe extinction effects no attempt was made to refine the structure.

Because the symmetry of the magnetic structure is monoclinic, reflections of the type $(h \frac{k}{2} \frac{l}{2})$ and $(h \frac{k}{2} \frac{l}{2})$ are not equivalent. The observed intensity distribution of the $(0 \frac{k}{2} \frac{l}{2})$ peaks showed that one of

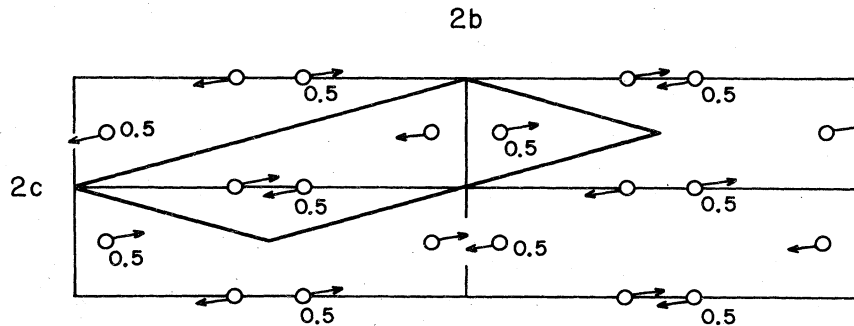


FIG. 4. Magnetic structure of BaMnF_4 projected on (100) showing one of the two equivalent domains. Small numerals denote heights of Mn atoms in the [100] direction. Monoclinic cell is shown in heavy outline. The antiferromagnetic axis is directed about 9° from the orthorhombic b axis towards doubled edge of monoclinic cell.

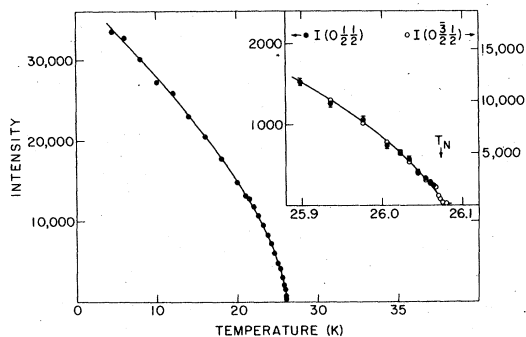


FIG. 5. Temperature dependence of integrated intensity of the $(0\frac{1}{2}\frac{1}{2})$ peak from BaMnF₄. The data near to T_N are shown in more detail in the inset, together with similar data for the $(0\frac{3}{2}\frac{1}{2})$ peak, normalized with respect to $(0\frac{1}{2}\frac{1}{2})$ at the lowest temperature range in this range.

the two structurally equivalent magnetic domains (defined as having $-\frac{k}{2} + \frac{l}{2} = 2n$) was about twice the volume of the other ($\frac{k}{2} + \frac{l}{2} = 2n + 1$).

The intensities of several magnetic peaks were measured as a function of temperature and found to disappear at about 26 K. No variation in the domain ratio could be detected, but significant extinction effects were observed in some of the stronger magnetic peaks. In $(0\frac{3}{2}\frac{1}{2})$ for example, extinction was already noticeable at 24.6 K. These scans were carried out in conventional fashion by rocking the crystal about the scattering vector. In the vicinity of the Néel point, however, this led to some problems in estimating

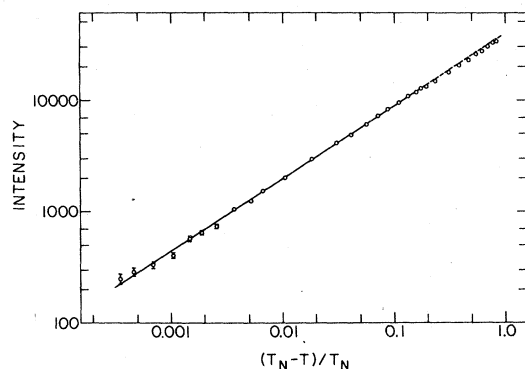


FIG. 6. Logarithmic plot of temperature dependence of integrated intensity of the $(0\frac{1}{2}\frac{1}{2})$ peak from the BaMnF₄ crystal. The solid line is a least-squares fit out to $(T_N - T)/T_N = 0.176$ ($T_N = 26.072$ K, $2\beta = 0.65$), the broken line being an extrapolation to lower temperatures. A fit to the data out to $(T_N - T)/T_N = 0.018$ gives $T_N = 26.076$ K, $2\beta = 0.70$.

background because of considerable amounts of critical scattering associated with the two-dimensional nature of the structure, which is characterized by the build-up of "rods" of diffuse scattering along the reciprocal b^* axis. The Bragg intensities of the $(0\frac{3}{2}\frac{1}{2})$ and $(0\frac{1}{2}\frac{1}{2})$ reflections were therefore measured in this region by performing scans along the line parallel to b^* at a distance $0.5c^*$ away, which enables the diffuse background to be properly determined. The intensities are plotted in Fig. 5, and very little three-dimensional critical scattering is seen to be present. A logarithmic plot of the intensity data against reduced temperature $(T_N - T)/T_N$ also demonstrates this, but rather surprisingly yields a critical exponent, 2β of 0.65 ± 0.03 (Fig. 6), characteristic of a three-dimensional system and in striking contrast to the much lower values obtained for BaCoF₄,³¹ and BaFeF₄.¹⁰

The intensity of the rod-like scattering was also studied by performing scans along the line parallel to c^* at a distance $-3.35b^*$ at several temperatures above T_N . A few of these are illustrated in Fig. 7, and the corresponding full widths at half maximum (FWHM) and the corresponding full widths at half maximum (FWHM) are plotted in Fig. 8 as a function of temperature. At about $2T_N$, which is roughly the temperature of the broad maximum in the magnetic susceptibility, the correlation length in the (010) planes is about 6 Å.

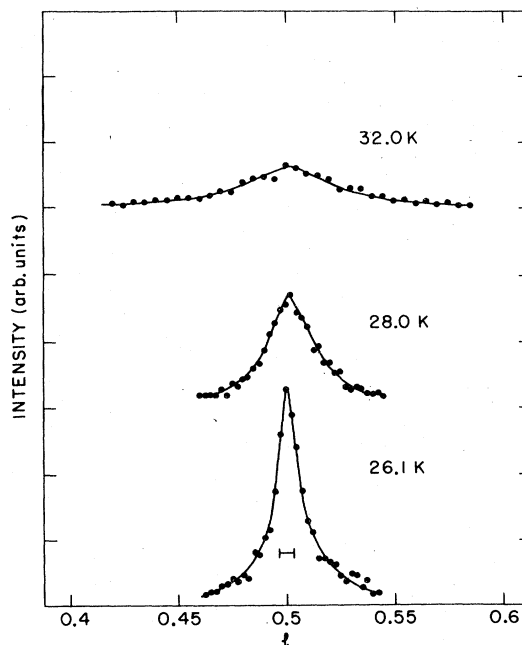


FIG. 7. Scans for BaMnF₄ crystal at selected temperatures above T_N in a direction $[0 -3.35 l]$, which is perpendicular to the reciprocal-lattice "rods."

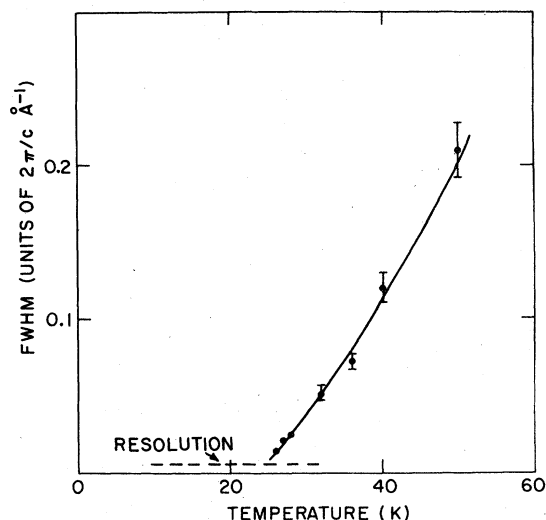


FIG. 8. Full-width at half-maximum of the peak at $(0, -3.35, 0.5)$ as a function of temperature.

III. MAGNETIC EXCITATIONS

A. Experimental

The magnetic excitations with wave vectors in the (ξ, η, η) plane of the reciprocal lattice were determined at 4.6 K. Since the primary magnetic reflection (see Sec. II) is $\vec{q}_M^M = (0, \pm 0.5, \pm 0.5)$, the magnetic Brillouin zone has $|\xi| \leq 0.5$ and $|\eta| \leq 0.25$. Within this Brillouin zone the magnetic excitations were determined for propagation directions along the high-symmetry directions $[\xi 00]$ and $[0\eta\eta]$ and the zone boundaries $(0.5, \eta, \eta)$ and $(\xi, 0.25, 0.25)$.

The measurements were performed with an incident energy of the neutrons of 14.7 meV and variable scattered energy. The horizontal collimation was 40 min in each part of the spectrometer, and a pyrolytic graphite filter was used to suppress higher-energy neutrons in the incident beam.

There are two branches of the spin-wave dispersion relation for spin waves propagating along the $[\xi 00]$ direction. Measurements of the upper branch were made largely for wave-vector transfer $\vec{Q} = (\xi, 0.5, 0.5)$ and for the lower branch for $\vec{Q} = (1 + \xi, 0.5, 0.5)$. The two branches of the spin waves propagating along $[0\eta\eta]$ were mainly determined with wave-vector transfer $\vec{Q} = (0, 0.5 + \eta, 0.5 + \eta)$ upper and $\vec{Q} = (1, 0.5 - \eta, 0.5 - \eta)$ lower.

The spin waves propagating along the two zone boundaries were determined with wave-vector transfers $\vec{Q} = (1 - \xi, 0.25, 0.25)$ and $\vec{Q} = (0.5, 0.5 - \eta, 0.5 - \eta)$. Some typical neutron

groups are shown in Fig. 9 and the results are summarized in Fig. 10. At the zone center the resolution of the spectrometer prohibited a reliable determination of the spin-wave excitation energy. The point shown in Fig. 10 was therefore obtained from the results of antiferromagnetic resonance measurements.¹⁵

B. Analysis of the magnetic excitations

The results shown in Fig. 10 were used to deduce the parameters of a simple model for the magnetic excitations in BaMnF_4 . The model adopted was to assume that there were Heisenberg exchange interactions between only the Mn ions lying within the sheets perpendicular to the b axis. We have not as yet explored this assumed two-dimensional nature of the spin waves because the present orientation of the crystal does not allow the observation of the spin waves propagating along the b axis.

Within the Mn-F planes two Heisenberg interactions were assumed: $H_{ij} = J_1(\vec{S}_i \cdot \vec{S}_j)$ between near-neighbor Mn ions along the zig-zagging a direction and $J_2(\vec{S}_i \cdot \vec{S}_j)$ for near neighbors along the c direction (Fig. 1). A single-ion anisotropy H_A was assumed to be constant at each site. With this model

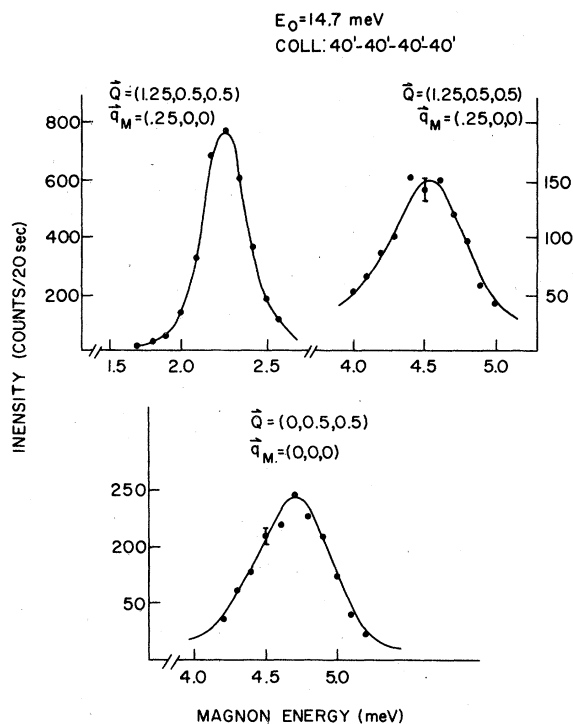


FIG. 9. Some typical neutron groups for magnetic excitations in BaMnF_4 crystal at 4.6 K.

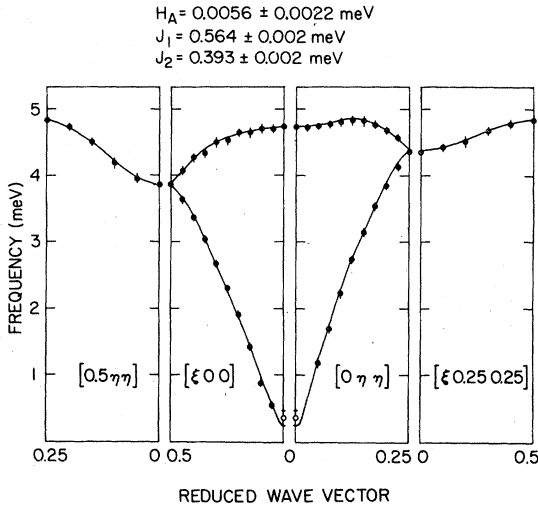


FIG. 10. Magnon dispersion curves for BaMnF₄ crystal at 4.6 K. The solid lines are a least-squares fit with $H_A = 0.0056$ meV, $J_1 = 0.393$ meV, and $J_2 = 0.564$ meV as described in the text.

the expressions for the magnetic excitations may be obtained from linear-spin-wave theory; the result is for $\vec{q} = (\xi, \eta, \eta)$

$$\omega(\vec{q}) = [A^2 - (B \pm C)^2]^{1/2}, \quad (1)$$

where

$$A = H_A + 2SJ_1 + 2SJ_2, \quad (2)$$

$$B = 2SJ_2 \cos(2\pi\eta),$$

and

$$C = 2SJ_1 \cos(\pi\xi).$$

This expression was fitted to the experimental results in a least squares sense to obtain the parameters H_A , J_1 , and J_2 . A good fit was obtained ($\chi^2 = 0.53$) as shown by the solid lines in Fig. 10, with the parameter values

$$H_A = 0.0056 \pm 0.0022 \text{ meV},$$

$$J_1 = 0.393 \pm 0.002 \text{ meV},$$

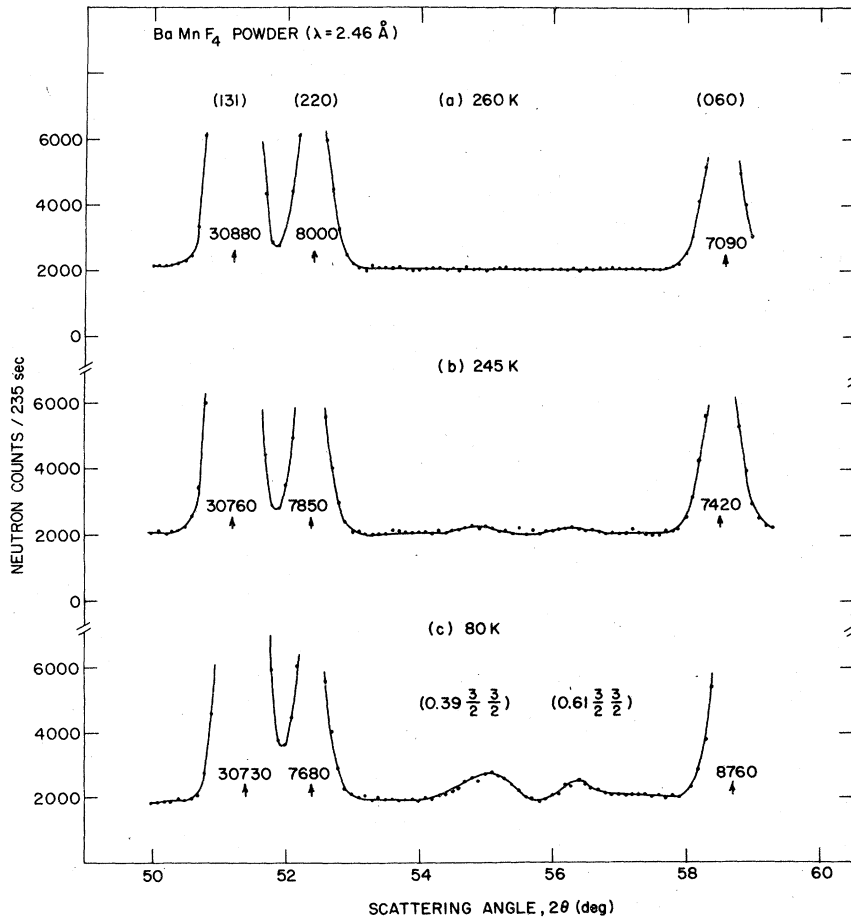


FIG. 11. Powder-neutron data from BaMnF₄ showing the behavior of the two weak superlattice peaks as a function of temperature (a) 260 K, (b) 245 K, (c) 80 K.

and

$$J_2 = 0.564 \pm 0.003 \text{ meV} .$$

The satisfactory fit obtained shows that the magnetic interactions are largely those assumed in our model.

Not surprisingly, the exchange constant between the spins along the zig-zagging a direction J_1 is smaller than that along the c direction: in the former case the superexchange path is bent but it is straight in the latter case. The magnitude of the exchange interactions along the c axis J_2 may be compared with the exchange constant found for Mn-F-Mn superexchange in other materials. In Rb_2MnF_4 the Mn-Mn distance is 4.21 Å and the exchange constant is 0.655 meV.³² This is surprisingly different from the value in BaMnF_4 considering the similarity of the Mn-Mn distance. The magnitude of the exchange J_2 is, however, consistent with the value ~ 0.5 meV calculated from the magnetic susceptibility.⁸

IV. STRUCTURAL PHASE TRANSITION

A. Elastic scattering

Following the confirmation of a structural phase transition,¹⁸ the two weak peaks in the powder diffraction pattern previously mentioned were studied in much more detail in the region of 250 K. Some of the data are shown in Fig. 11 and it is clear that both peaks are absent at 260 K. The intensity of the stronger is plotted as a function of temperature in Fig. 12, and is seen to vanish slightly above 250 K. There is no doubt, therefore, that the two peaks are superlattice reflections associated with the structural transition. However, all attempts at indexing including a computer search involving multiple cells with edges up to three times those of the chemical cell, were completely unsuccessful. Profile refinement of data collected at 260, 245, and 80 K were carried out as before, excluding the two extra peaks where appropriate. In order to make some allowance for a change in temperature factors, an additional negative overall B was included, but otherwise all structural parameters were fixed at the Keve *et al.*⁵ values. Results are listed in Table I, and observed and calculated intensities in Table IV. Inspection of Table IV reveals no significant changes in observed intensities as a function of temperature, with the possible exception of the (060) reflection.

The refined values of the orthorhombic cell dimensions and volumes are plotted against temperature in Fig. 13. There are no obvious discontinuities, but the absence of any perceptible change in a over most of the range is anomalous.

A search for one of the two small superlattice peaks observed in the powder pattern was carried out

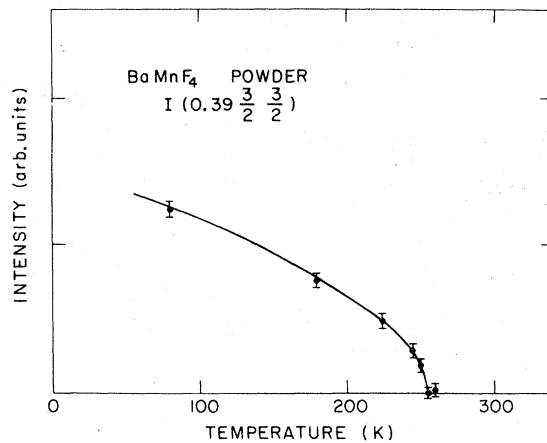


FIG. 12. Temperature dependence of integrated intensity of the stronger of the superlattice peaks shown in Fig. 11.

on a second, larger single crystal (dimensions roughly $5 \times 5 \times 10 \text{ mm}^3$). Considerable effort was devoted to this, but even so, it was probably very fortunate that one of these peaks was ever discovered since the peaks appear unexpectedly at an incommensurate position in reciprocal space. Figure 14 shows that the most intense superlattice reflections were observed at

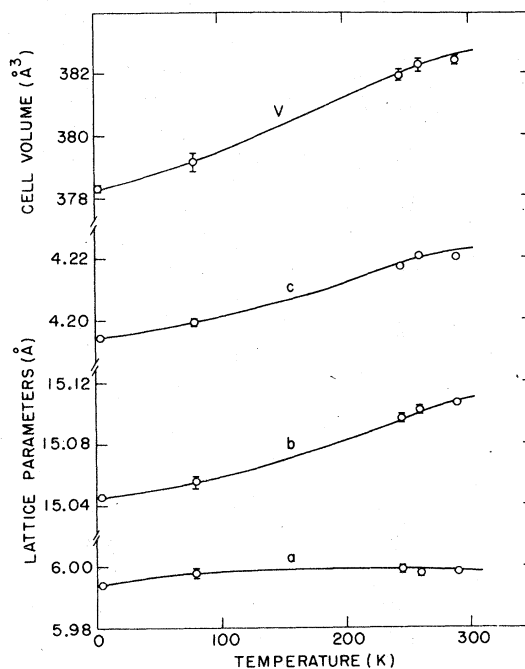


FIG. 13. Least-squares values of lattice parameters and cell volumes from profile refinement of BaMnF_4 powder data as a function of temperature. The solid lines are a guide for the eye.

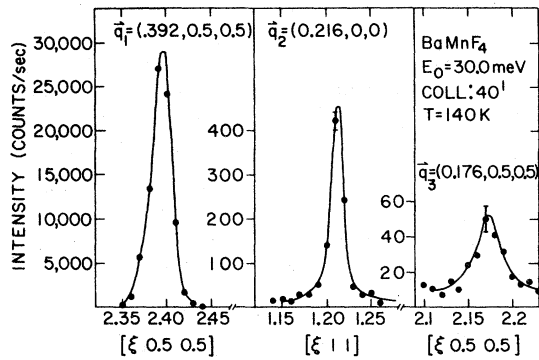


FIG. 14. Superlattice peaks at $T = 140$ K at $\bar{q}_1 = (\pm 0.392, \pm 0.5, \pm 0.5)$, $\bar{q}_2 = (\pm 0.216, 0, 0)$ and $\bar{q}_3 = (0.176, \pm 0.5, \pm 0.5)$ corresponding to the primary and secondary order parameters.

the reduced wave vector

$$\bar{q}_1 = (\pm 0.392, \pm 0.5, \pm 0.5)$$

Additional superlattice peaks were observed at

$$\bar{q}_2 = (\pm 0.216, 0, 0)$$

and

$$\bar{q}_3 = (0.176, \pm 0.5, \pm 0.5)$$

with decreasing intensity as shown in Fig. 14. The

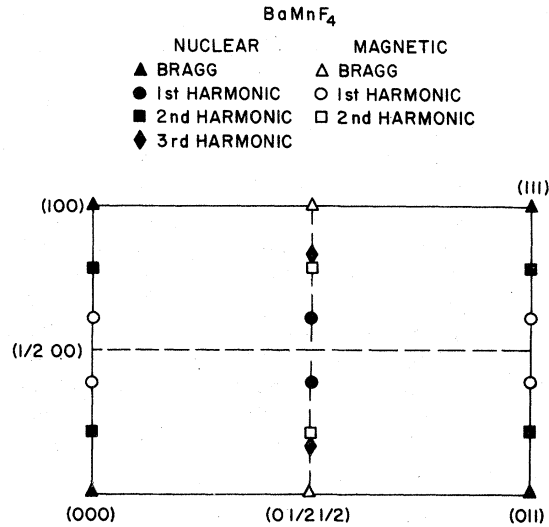


FIG. 15. Schematic representation of the positions in reciprocal space of observed superlattice peaks associated with the structural phase transition (filled symbols) and magnetic phase transition (open symbols).

satellite positions are related to each other as follows: $\bar{q}_2 = 2\bar{q}_1$ and $\bar{q}_3 = 3\bar{q}_1$, when reduced to the first Brillouin zone. Figure 15 gives a schematic representation of the position in reciprocal space of nuclear Bragg peaks and superlattice peaks. A surprising

TABLE IV. Comparison of observed and calculated nuclear intensities from polycrystalline BaMnF₄ at 260, 245, and 80 K. Parameters as in Table I. Scattering lengths as in Table II.

$h k l$	260 K		245 K		80 K	
	I_{calc}	I_{obs}	I_{calc}	I_{obs}	I_{calc}	I_{obs}
0 2 0	24	26	24	25	24	23
1 2 0	49	58	49	58	50	60
0 1 1	3	1	3	2	3	3
0 4 0	1	3	1	1	1	2
1 1 1	0	0	0	0	0	1
0 3 1	1	1	1	1	1	1
1 4 0	9	9	9	9	9	9
2 0 0	20	23	20	23	20	25
1 3 1	221	212	220	208	227	211
2 2 0	38	44	38	44	39	43
0 6 0	48	44	48	49	50	64
0 5 1	186	165	185	167	193	174
2 1 1	354	384	354	384	371	395
1 5 1	269	243	269	244		
2 3 1	269	271	244	272		
0 0 2	135	135	135	131		

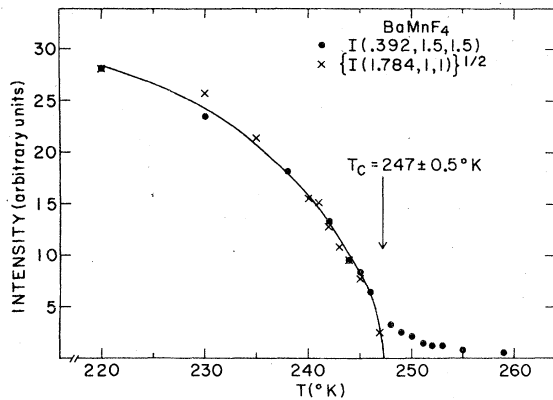


FIG. 16. $I(\bar{q}_1)$ and $[I(\bar{q}_2)]^{1/2}$ vs temperature.

feature of this incommensurate phase is that the satellite positions show no temperature dependence in contrast to the incommensurate phases in metallic systems such as TaSe₂ and NbSe₂,³³ and ferroelectric incommensurate materials such as K₂SeO₄.³⁴

The intensities of the \bar{q}_1 , \bar{q}_2 , and \bar{q}_3 satellites also are related. Figure 16 shows the temperature dependence of the intensity of the \bar{q}_1 -type satellite and the square root of the intensity of a \bar{q}_2 -type reflection normalized to each other at low temperature. From

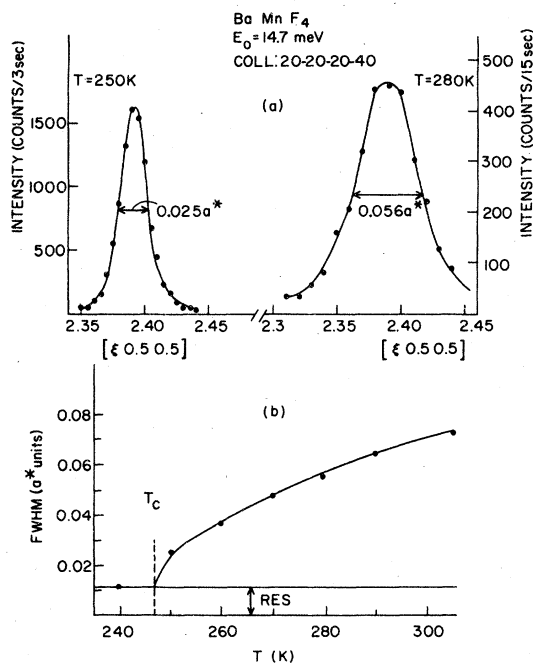


FIG. 17. Temperature dependence of the line width of a \bar{q}_1 satellite above T_c . The top part shows two profiles at different temperatures. The bottom shows the temperature dependence of the FWHM. ($a^* = 1.045 \text{ \AA}^{-1}$.)

this figure we conclude the $I(\bar{q}_1)$ is approximately proportional to $[I(\bar{q}_2)]^{1/2}$. Since no critical scattering appears at $I(\bar{q}_2)$ it is more reasonable to use this reflection to obtain the critical index β of the order parameter. From a log-log plot of $I(\bar{q}_2)$ against $T_c - T$ with $T_c = 247.0 \pm 0.5 \text{ K}$, we obtain a value for β [from the relationship $I(\bar{q}_2) \propto (T_c - T)^{4\beta}$] of 0.31 ± 0.05 . The intense critical scattering observed at $I(\bar{q}_1)$ implies that the intensities at \bar{q}_1 provide a measure of the fluctuations of the primary order parameter associated with the structural phase transition.

The observed satellites at \bar{q}_2 and \bar{q}_3 , respectively, could possibly result from double and triple reflections involving successive \bar{q}_1 satellites. To investigate this possibility, the behavior of a number of \bar{q}_2 reflections was studied as a function of incident energy in the range 4.4–5.3 meV and 13.0–15.0 meV, and also as a function of rotation about the scattering vector. Erratic results were obtained in a few cases, but in general the intensity behavior was not characteristic of the presence of strong multiple scattering effects. We therefore conclude that multiple scattering is not the origin of the \bar{q}_2 satellites. These can be explained either as diffraction harmonics of the nearly sinusoidal distortions with wave vector \bar{q}_1 or secondary distortions of the high-temperature structure. Over 40 different \bar{q}_1 superlattice reflections were measured in an attempt to identify the distortions occurring in the low-temperature structure. Thus far, we have been unsuccessful in obtaining a good physical picture of the atomic displacements necessary to produce the incommensurability of 0.392 along a^* .

The critical scattering is observed over a large range of temperatures above T_c . Figure 17 shows Q scans of the satellite $\bar{Q}_1 = (2.39, 0.5, 0.5)$ along the $[\xi 00]$ direction. The width is seen to increase for the higher temperatures. In the lower part of the figure we plot the temperature dependence of the full width at half maximum (FWHM) in terms of a^* units ($a^* = 1.045 \text{ \AA}^{-1}$). At the highest temperatures measured ($T = 305 \text{ K}$) the line width is much broader than the resolution and corresponds to a correlation length of approximately 30 \AA .

At low temperatures, the Mn ions are displaced from their high-temperature positions as a result of the incommensurate lattice distortion. This will cause new magnetic satellites to appear at positions relative to the new reciprocal lattice of the low-temperature incommensurate phase. This is shown schematically in the reciprocal space diagram of Fig. 15. For example, relative to the high-temperature structure, the fundamental magnetic superlattice peaks appear at $\bar{q} = (0, 0.5, 0.5)$ points in reciprocal space as discussed in Sec. II A. Other magnetic peaks relative to the $(0.39, 0.5, 0.5)$ incommensurate nuclear lattice will appear as a first harmonic at $(0.39, 0, 0)$, and the second harmonic at $(0.78, 0.5, 0.5)$

corresponding to the harmonics of the nuclear structure.

The discrepancies in the observed and calculated powder magnetic intensities for the structure with moments directed along the b axis described in Sec. II A could conceivably originate from the displacements of the Mn ions in the incommensurate structure. However, the intensities of the \bar{q}_1 magnetic satellites are typically three to four orders of magnitude less than those of the primary magnetic reflections, from which it may be inferred that the Mn displacements are very small and not likely to have any detectable effect on the primary peaks. This inference is supported by the nuclear intensity data in Table IV, where it can be seen that the intensities of the fundamental reflections are essentially unchanged, although in this case the \bar{q}_1 nuclear satellites are typically only one to two orders of magnitude smaller. It is therefore more plausible to attribute the intensity discrepancies to a small deviation of the antiferromagnetic axis from the b axis, as already discussed.

B. Normal modes of vibration in BaMnF₄

Above the structural phase transition, inelastic neutron scattering measurements were performed to examine the normal modes of vibration with wave vectors close to the incommensurate superlattice wave vector $\bar{q}_1 = (0.39, 0.5, 0.5)$, in order to determine if the transition is caused by a softening of one of these normal modes. The crystal used was a large cylindrical boule, about 17 mm in diameter and 30-mm long. The measurements were performed under a variety of conditions with incident neutron energies of 5.0, 14.7, and 30.0 meV. Since the scattering was found to be largely quasielastic in character, the measurements were made difficult by the presence of the intense paramagnetic scattering from the Mn²⁺ spins, especially for smaller wave-vector transfer.

Energy scans were performed at a variety of temperatures to study the modes with propagation directions $[\xi 0.5 0.5]$ and $[0.39 \eta \eta]$. The most successful measurements were performed near the wave vector $\bar{Q} = (4.61, 1.5, 1.5)$ with an incident energy of 30.0 meV. This large wave vector was chosen so that the wave-vector dependence of the Mn²⁺ form factor drastically reduced the magnetic scattering. Figure 18 shows examples of constant \bar{Q} scans at $\bar{Q} = (4.61, 1.5, 1.5)$ for several temperatures. The spectra show a broadened quasielastic peak whose width decreases as $T \rightarrow T_c$ and is resolution limited below 300 K. Figure 19 shows the reciprocal of this intensity, multiplied by temperature for these scans. This quantity decreases towards zero approximately linearly with $(T - T_c)$ from a temperature of 581 K down to T_c . This behavior is typical of other systems

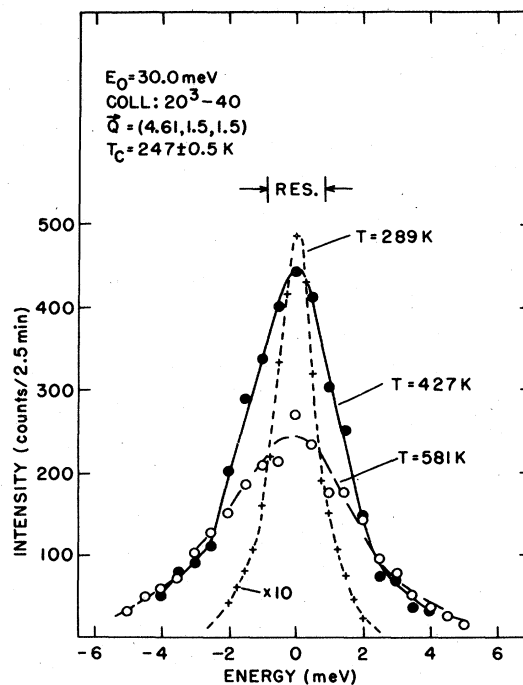


FIG. 18. Low-energy resolution scans of the mode associated with the structural phase transition in BaMnF₄ at several temperatures above T_c .

where the soft mode is overdamped.³⁵

The soft-mode branch becomes underdamped as $0.39 - \xi$ increases. Figure 20 shows scans along the $[\xi 0.5 0.5]$ direction at $T = 581$ K for $\xi = 0.30, 0.35$, and 0.39 . At $\xi = 0.39$, the mode is overdamped, but has a width larger than the resolution. As ξ decreases a propagating feature begins to emerge. For the $[0.39 \eta \eta]$ direction, the mode becomes more rapidly underdamped as η changes and is relatively in-

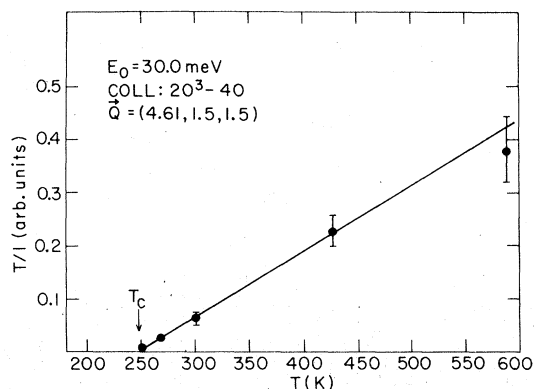


FIG. 19. Reciprocal of the intensity of the neutron scattering multiplied by temperature for the mode associated with the structural phase transition in BaMnF₄.

sensitive to temperatures for $\xi \leq 0.35$. Figure 21 is a plot of the dispersion of the soft-mode branch along the $[\xi 1.5 1.5]$ and $[0.39 \eta \eta]$ directions at 300 K. The measured spectra can be fit with the cross section for scattering off a damped harmonic oscillator.

$$S(\vec{Q}, \omega) = [n(\omega) + 1] \frac{A \omega \gamma}{(\omega_0^2 - \omega^2)^2 + \omega^2 \gamma^2} \quad (3)$$

where ω_0 is the frequency of the phonon, γ is the damping, $n(\omega)$ is the thermal occupation factor, and A is the normalization constant. Within the dotted region of Fig. 21, the mode is overdamped but the above formalism can still be used except for wave vectors very near \vec{q}_1 where a divergent central peak is present. This is shown in the high-resolution spectra of Fig. 22 taken at $\vec{Q} = (2.39, 0.5, 0.5)$. On the energy scale of this figure, the broad background is the overdamped soft mode and the narrow, resolution limited central peak at $\hbar\omega = 0$ is seen to diverge as the transition temperature, $T_c = 247.5$ K is approached. This feature is very similar to that observed in KMnF_3 ,³⁶ where a central peak is observed in addition to an overdamped soft mode. The major difference of course is that in KMnF_3 the wave vector of the fluctuations of the order parameter is commensurate at $(0.5, 0.5, 0.5)$ whereas in BaMnF_4 , it is incommensurate.

Experiments below T_c were made difficult by the paramagnetic scattering which increases as T is lowered. The shapes of the dispersion curves of Fig.

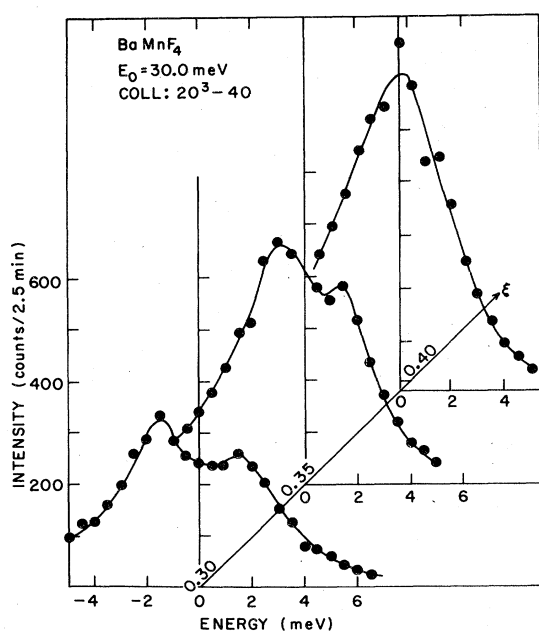


FIG. 20. Spectral profiles for the soft-mode branch propagating along the $[\xi 0.5 0.5]$ direction at $T = 581$ K.

21 away from \vec{q}_1 do not substantially change except for a slight increase in frequency as T decreases. Scans about the point \vec{q}_1 were performed to search for any additional modes which could be related to amplitude or phase fluctuations, but none was found.

V. THEORY OF STRUCTURAL PHASE TRANSITION

A. Ginzburg-Landau theory

As seen above, the low-temperature phase of BaMnF_4 is one in which the high-temperature structure is modulated by a distortion with a wave vector which is incommensurate with the lattice $\vec{q}_1 = (0.39, 0.5, 0.5)$. Because the theory of such transitions is not well understood and certainly not widely known, we discuss the theory for BaMnF_4 in some detail. The symmetry of the high-temperature phase⁵ of BaMnF_4 , $A2_1am$, is such that the "small" representation of the wave vector $(\zeta, 0.5, 0.5)$ is one-dimensional.³⁷ There are then four different but equivalent wave vectors which describe the primary

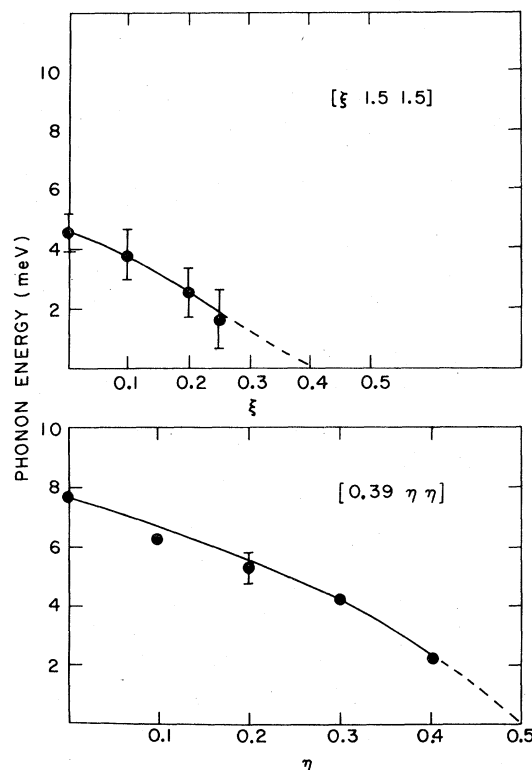


FIG. 21. Frequencies of the excitations in BaMnF_4 propagating along the directions $[\xi 1.5 1.5]$ and $[0.39 \eta \eta]$ at $T = 300$ K. Within the dotted region the modes are overdamped.

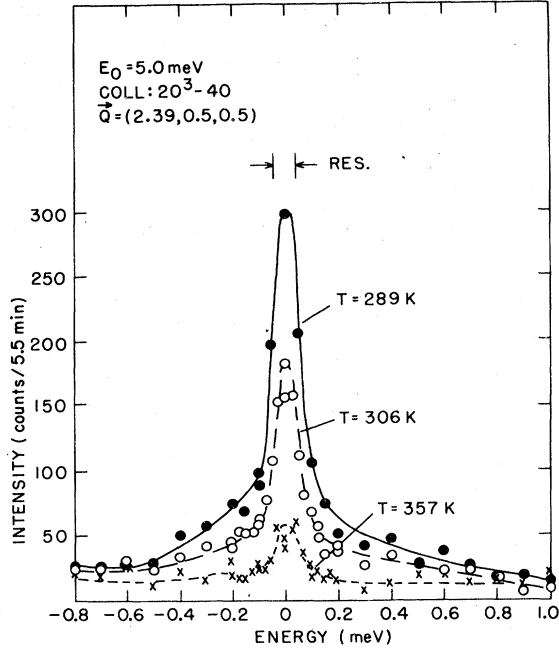


FIG. 22. High-resolution measurements of the nearly elastic scattering from the mode associated with the structural phase transition in BaMnF₄. Note that there is a resolution limited quasielastic component whose intensity is growing rapidly as $T - T_c$.

order parameters

$$\bar{q}_1 = (0.39, 0.5, 0.5), \quad \bar{q}_2 = -\bar{q}_1,$$

$$\bar{q}_3 = (0.39, -0.5, 0.5), \quad \bar{q}_4 = -\bar{q}_3.$$

In addition, experiment and theory show that the primary order parameters couple to secondary order parameters; the elastic strains²⁰ and distortions with wave vectors

$$\bar{q}_5 = (0.78, 0, 0), \quad \bar{q}_6 = -\bar{q}_5,$$

$$\bar{q}_7 = (0.78, 1, 0), \quad \bar{q}_8 = -\bar{q}_7,$$

as shown in Fig. 14.

The inclusion of these parameters in the theoretical development considerably complicates the formalism. We therefore include in the text only the development neglecting the effects of the secondary order parameters. The theory has been calculated including their effects with qualitatively similar but lengthier expressions for the frequencies and amplitudes of the distortions.

In the Landau theory of phase transitions the free energy of the crystal is expanded in a power series in the order parameters. Neglecting the secondary order parameters and including terms only up to fourth order in the displacements the expansion for BaMnF₄

is

$$F_L = A(Q_1 Q_2 + Q_3 Q_4) + V_1(Q_1^2 Q_2^2 + Q_3^2 Q_4^2) + V_2 Q_1 Q_2 Q_3 Q_4 + V_3 Q_1^2 Q_2^2 + V_3^* Q_3^2 Q_4^2, \quad (4)$$

where the coefficient A is normally written $A = a(T - T_c)$, while V_1 and V_2 are real coefficients associated with normal scattering processes, and $V_3 = V e^{i\alpha}$ with V positive describes an umklapp scattering process. The amplitudes of the four different primary order parameters are written Q_1, \dots, Q_4 , respectively.

Since the displacements of the atoms at the transition are real, the distortions at the phase transition must be of the form

$$Q_1 = \phi_1 e^{i\psi_1}, \quad Q_3 = \phi_2 e^{i\psi_2},$$

$$Q_2 = \phi_1 e^{-i\psi_1}, \quad Q_4 = \phi_2 e^{-i\psi_2},$$

where $\phi_{1,2}$ and $\psi_{1,2}$ are real. When these are substituted into Eq. (4), the result is

$$F_L = A(\phi_1^2 + \phi_2^2) + V_1(\phi_1^4 + \phi_2^4) + V_2 \phi_1^2 \phi_2^2 + 2V \phi_1^2 \phi_2^2 \cos(\alpha + 2\psi_1 - 2\psi_2). \quad (5)$$

Differentiating this expression to give the stability conditions yields

$$A + 2\phi_1^2 V_1 + V_2 \phi_2^2 + 2V \phi_2^2 \cos(\alpha + 2\psi_1 - 2\psi_2) = 0,$$

$$A + 2\phi_2^2 V_1 + V_2 \phi_1^2 + 2V \phi_1^2 \cos(\alpha + 2\psi_1 - 2\psi_2) = 0, \quad (6)$$

$$V \phi_1^2 \phi_2^2 \sin(\alpha + 2\psi_1 - 2\psi_2) = 0.$$

From the third of these equations, the relative phases of the order parameters are defined through the umklapp term.

There are two possible solutions below T_c which have continuous phase transitions at T_c . Solution (i) has $\phi_1 = \phi_2 = \phi$ with

$$\phi^2 = \frac{a(T_c - T)}{2V_1 + V_2 - 2V} \quad (7)$$

and

$$F_L = -\frac{A^2}{2V_1 + V_2 - 2V}.$$

Solution (ii) has $\phi_1 = \phi, \phi_2 = 0$ with

$$\phi^2 = \frac{a(T_c - T)}{2V_1}, \quad (8)$$

and

$$F_L = -\frac{A^2}{4V_1}.$$

Solution (i) will be stable if

$$0 < 2V_1 + V_2 - 2V < 4V_1, \quad (9)$$

while solution (ii) will be stable if

$$0 < 4V_1 < 2V_1 + V_2 - 2V \quad (10)$$

Since it is impossible to calculate these coefficients from first principles we do not know which is the stable solution. Purely on the statistics of random numbers, however, it is more likely that solution (i) will be the stable solution. In part this is because in that solution the relative phase angles may be chosen so that the effect of the umklapp term is to stabilize

the ordered phase by choosing

$$\alpha + 2\psi_1 - 2\psi_2 = (2n + 1)\pi \quad (11)$$

The frequencies of the normal modes can be obtained by treating the free energy [Eq. (4)] in a Landau-Ginzburg sense, and identifying above T_c , $A = \omega^2$.

Below T_c the four modes for solution (i) have frequencies and eigenvectors (Q_1, Q_2, Q_3, Q_4) given by

$$\begin{aligned} \omega_1^2 &= 2a(T_c - T), \quad \bar{e}_1 = \frac{1}{2}(e^{i\psi_1}, e^{-i\psi_1}, e^{i\psi_2}, e^{-i\psi_2}), \\ \omega_2^2 &= a(T_c - T) \frac{4V_1 - 2V_2 + 4V}{2V_1 + V_2 - 2V}, \quad \bar{e}_2 = \frac{1}{2}(e^{i\psi_1}, e^{-i\psi_1}, -e^{i\psi_2}, -e^{-i\psi_2}), \\ \omega_3^2 &= a(T_c - T) \frac{8V}{2V_1 + V_2 - 2V}, \quad \bar{e}_3 = \frac{1}{2}(e^{i\psi_1}, -e^{-i\psi_1}, e^{i\psi_2}, -e^{-i\psi_2}), \\ \omega_4^2 &= 0, \quad \bar{e}_4 = \frac{1}{2}(e^{i\psi_1}, -e^{-i\psi_1}, -e^{i\psi_2}, e^{-i\psi_2}). \end{aligned} \quad (12)$$

These four modes have fairly simple physical interpretations. The first two are amplitude modes and correspond to oscillations of the amplitudes ϕ_1 and ϕ_2 . In mode (a) these oscillations are in phase and in mode (b) out of phase. Note that the frequency of mode (a), the totally symmetric mode, is given by the same expression as its frequency in the Landau-Ginzburg theory of commensurate phase transitions.

The third and fourth modes are oscillations of the phases ψ_1 and ψ_2 . In mode (c) these oscillations are out of phase and the frequency of the mode is determined by the umklapp terms in the free-energy expansion. In the fourth mode the phase motions are in phase and this motion costs no energy so that the mode is the Goldstone boson corresponding to the continuous phase symmetry of the incommensurate phase.

If the low-temperature phase has the alternative crystal structure [solution (ii)] the frequencies of the modes and their eigenvectors are given by

$$\begin{aligned} \omega_1^2 &= 2a(T_c - T), \quad \bar{e}_1 = \frac{1}{2^{1/2}}(e^{i\psi_1}, e^{-i\psi_1}, 0, 0), \\ \omega_2^2 &= 0, \quad \bar{e}_2 = \frac{1}{2^{1/2}}(e^{i\psi_1}, -e^{-i\psi_1}, 0, 0), \\ \omega_3^2 &= a(T_c - T) \left[\frac{V_2 + 2V - 2V_1}{2V_1} \right], \quad \bar{e}_3 = \frac{1}{2^{1/2}}(0, 0, 1, e^{-i(\alpha + 2\psi_1)}), \\ \omega_4^2 &= a(T_c - T) \left[\frac{V_2 - 2V - 2V_1}{2V_1} \right], \quad \bar{e}_4 = \frac{1}{2^{1/2}}(0, 0, 1, -e^{-i(\alpha + 2\psi_1)}). \end{aligned} \quad (13)$$

The first of these modes is the normal amplitude mode corresponding to oscillations of ϕ , and the second the zero-energy phase mode corresponding to oscillations of ψ_1 . The third and fourth modes are the amplitude and phase modes associated with the wave vectors \bar{q}_3 and \bar{q}_4 . This phase has been analyzed assuming that the distorted phase is associated with the wave vectors \bar{q}_1 and \bar{q}_2 . There is an exactly equivalent solution with wave vectors \bar{q}_3 and \bar{q}_4 interchanged with \bar{q}_1 and \bar{q}_2 . In a bulk crystal both of these domains are likely to be present, probably in roughly equal proportions.

In a neutron scattering experiment below T_c , both distorted structures give rise to the result that four

modes should be observed for a wave-vector transfer of the form $\bar{Q} = \bar{\tau} + \bar{q}_1$, where $\bar{\tau}$ is a reciprocal lattice vector of the high-temperature phase. Because all of the modes have the same amplitude the intensities of the modes differ only because of the explicit frequency dependent factors in the cross section, which is given by

$$S(\bar{Q}, \omega) = K(\bar{Q}) \sum_{i=1}^4 \frac{n(\omega_i) + 1}{\omega_i} \delta(\omega - \omega_i), \quad (14)$$

where $K(\bar{Q})$ is a constant. Above the phase transition only one mode is observable for each wave vector and its intensity is given by Eq. (3) with $\omega_0^2 = a(T - T_c)$.

In contrast, in a Raman scattering experiment only the fully symmetric amplitude mode is observable below T_c and none is observable above T_c .

These results are applicable only for wave-vector transfers corresponding to the new Bragg reflections. For neighboring wave vectors, the frequencies of the modes are expected to rise with increasing wave vector from the Bragg reflection, quadratically with the wave vector for all the modes except for the Goldstone phase modes whose frequencies rise linearly with increasing wave vector.

B. Critical phenomena

The phase transition in BaMnF₄ has four primary order parameters. It is therefore an example of an $n = 4$ model of the type which has recently been discussed by Mukamel³⁸ and by Mukamel and Krinsky.³⁹ In order to discuss the critical phenomena it is

$$\begin{aligned} \mathcal{H} = & +\frac{1}{2} \sum_{i=1}^2 u_2(\bar{q})(P_i^2 + \bar{P}_i^2) + u \sum_{i=1}^2 (P_i^2 + \bar{P}_i^2)^2 + v(P_1^2 + \bar{P}_1^2)(P_2^2 + \bar{P}_2^2) \\ & + w[(P_1^2 - \bar{P}_1^2)(P_2^2 - \bar{P}_2^2) + 4P_1\bar{P}_1P_2\bar{P}_2] , \end{aligned} \quad (16)$$

where we have used the conventional notation of renormalization-group theory and suppressed the summations over the various integrals. In terms of the earlier notation, Eq. (4),

$$u_2(\bar{q}) = A + q^2, \quad u = V_1/4, \quad (17)$$

$$v = V_2/4, \quad w = V_3/2,$$

with the phases of the eigenvectors of the u modes chosen so that $\alpha = n\pi$.

The Hamiltonian Eq. (16) is very similar to that considered by Mukamel and Krinsky, apart from the additional w term.

The critical properties of the Hamiltonian have been investigated using the techniques of renormalization-group theory.⁴⁰ In dimension $d = 4 - \epsilon$, keeping only terms of order ϵ and assuming a small momentum cutoff of b^{-1} , the recursion relations become

$$\begin{aligned} u' &= b^\epsilon [u - (40u^2 + 2v^2 + 2w^2)K_4 \ln b] , \\ v' &= b^\epsilon [v - (32uv + 8v^2 + 16w^2)K_4 \ln b] , \\ w' &= b^\epsilon [w - 16w(u + v)K_4 \ln b] , \end{aligned} \quad (18)$$

where $K_4 = 1/8\pi^2$.

These recursion relations have the following fixed

necessary to extend the Landau expression for the free energy to construct an effective Hamiltonian for all the modes in the neighborhood of the ordering wave vector. This effective Hamiltonian can be written in a form more closely allied to that of Mukamel and Krinsky if the variables are changed by the transformation

$$\begin{aligned} Q_1(\bar{q}_1 + \bar{q}) &= \frac{1}{2^{1/2}} [P_1(\bar{q}) + i\bar{P}_1(\bar{q})] , \\ Q_2(\bar{q}_2 + \bar{q}) &= \frac{1}{2^{1/2}} [P_1(\bar{q}) - i\bar{P}_1(\bar{q})] , \\ Q_3(\bar{q}_3 + \bar{q}) &= \frac{1}{2^{1/2}} [P_2(\bar{q}) + i\bar{P}_2(\bar{q})] , \\ Q_4(\bar{q}_4 + \bar{q}) &= \frac{1}{2} [P_2(\bar{q}) - i\bar{P}_2(\bar{q})] , \end{aligned} \quad (15)$$

when the effective Hamiltonian becomes

points: (i) the Gaussian fixed point

$$u^* = v^* = w^* = 0, \quad (19)$$

(ii) three equivalent fixed points corresponding to two independent $n = 2$ systems

$$u^* = \frac{\epsilon}{40K_4}, \quad v^* = w^* = 0 \quad (20)$$

$$u^* = \frac{\epsilon}{80K_4}, \quad v^* = \frac{\epsilon}{20K_4}, \quad w^* = \pm \frac{\epsilon}{40K_4},$$

and (iii) the isotropic $n = 4$ fixed point

$$u^* = \frac{\epsilon}{48K_4}, \quad v^* = 2u^*, \quad w^* = 0. \quad (21)$$

The first of these fixed points is unstable against all perturbations.

The stability of the second and third fixed points requires more consideration. In the absence of the w term in the Hamiltonian [Eq. (16)], a nonperturbative renormalization-group argument⁴¹ suggests that for $d = 3$ the stable fixed point is that for two $n = 2$ independent systems, and that the $n = 4$ isotropic fixed point is unstable. This conclusion is at variance with that of Mukamel.³⁸

The introduction of the w perturbation in the Ham-

iltonian then makes the $n = 2$ fixed point unstable. Since to order (ϵ) , no new fixed points are introduced, there are no stable fixed points to the recursion relations and hence it may be presumed that the phase transition is one of the class of phase transitions which are driven to be first order by the critical fluctuations as discussed for other $n \geq 4$ systems.^{39,42}

It is of some interest to discuss the nature of the phase diagram as the ordering wave vector varies along the $[\xi 0.5 0.5]$ direction. It is convenient to write the expression for the quadratic term $u_2(\vec{q})$ as a function of ξ in the form

$$u_2(\vec{q}) = B + A \left(\frac{1}{4} \cos 4\pi\xi + \beta \cos 2\pi\xi \right) \quad (22)$$

This expression for $A > 0$ has a minimum for $\xi = 0$, if $\beta < -1$, and for $\xi = 0.5$, if $\beta > 1$. For intermediate values of β the expression has a minimum for $\xi = \xi_0$, where $\cos 2\pi\xi_0 = -\beta$. In Fig. 23 we show schematic form of the phase diagram as evaluated within mean-field theory by using the expression (22) for $u_2(\vec{q})$, and neglecting higher harmonics of the order parameter. In principle, within mean-field theory, it is possible for the wave vector ξ_0 to lock into any wave vector of the form $\xi_0 = (n_1/n_2)0.5$, where n_1 and n_2 are integers. In practice the lock-in energy appears to be unimportant if n_2 is larger than 2. In Fig. 23 we have therefore only indicated a lock-in occurring for $\xi_0 = 0.25$.

The points A and B in the phase diagram are

known as Lifshitz points, and occur when the parameter $\beta = -1, A$, or $\beta = +1, B$. For these values of β the second derivative of the dispersion relation, Eq. (22) is zero at the minima of the dispersion relations.

The form of this phase diagram has not been evaluated in detail including the effects both of the higher harmonics of the order parameter⁴³ and the critical fluctuations. The nature of the transitions from the undistorted high-temperature phase into the various distorted phases may however be outlined. Firstly, the transition into the incommensurate phase is expected to be driven to be first order by the critical fluctuations. The transition to the commensurate phase with $\xi_0 = \frac{1}{4}$, can also be shown to be of first-order character.

The transition to the commensurate phases with $\xi_0 = 0$ or 0.5 , are both described by Hamiltonians which are of the general $n = 2$ form. The transitions to these phases are therefore expected to be continuous and belong to the universal class of isotropic $n = 2, d = 3$ system. The renormalization-group theory of Lifshitz points has been described by Hornreich *et al.*⁴⁴ Unfortunately they do not give the results for our particular case, a uniaxial Lifshitz point of an $n = 2$ system. It is reasonable, however, to expect and is confirmed by detailed calculation that the exponents will be not too different from those of a uniaxial Lifshitz point of an $n = 1$ system for which, to lowest order in ϵ , the exponents describing

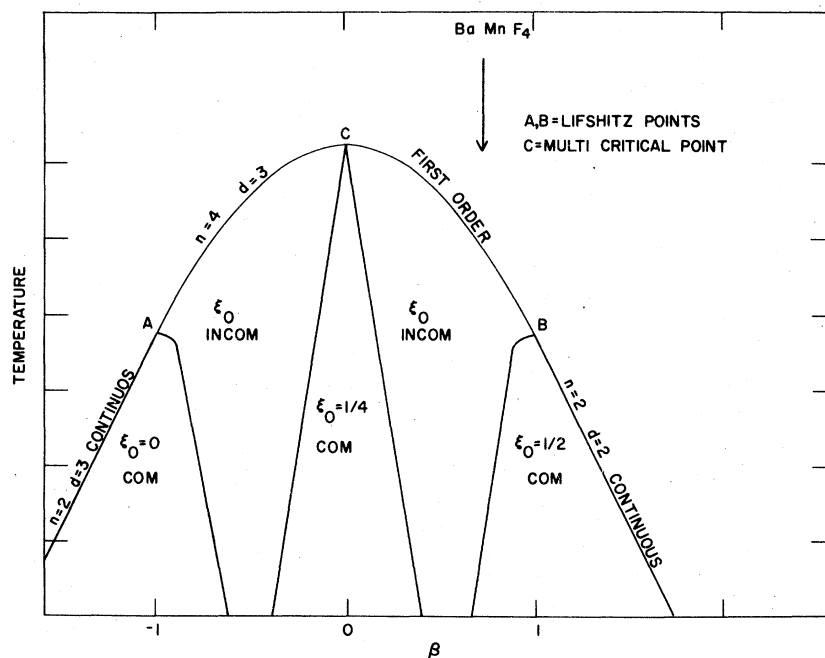


FIG. 23. Schematic representation of the phase diagram for distortions of the wave vector $(\xi_0, 0.5, 0.5)$ as determined by the parameter β of Eq. (22). The form of the lines has been calculated only within mean-field theory.

the temperature dependence of the order parameter and susceptibility, β and γ , are 0.25 and 1.25, while that describing the correlations along the $[\xi, 0.5, 0.5]$ direction, ν is 0.31.

C. Comparison with experiment

The measured value of β , the critical exponent of the temperature dependence of the order parameter Fig. 16 is $\beta = 0.31 \pm 0.05$. This is significantly different from the value of $\beta = 0.5$ as expected from the Landau theory discussed above. However, as we have shown, the critical fluctuations are expected to drive the phase transition first order (see Fig. 23). We have not as yet observed any discontinuity, but this small value of the exponent is the result of the order parameter decreasing more rapidly than is normally found. This type of behavior occurs even more extremely at a first-order phase transition. It is also worth noting that the dispersion relation along the $[\xi, 0.5, 0.5]$ direction is relatively flat (Fig. 21). Consequently, the system is very close to the Lifshitz point associated with the critical values of the dispersion relation when the phase transition changes from a continuous $n = 2$ phase transition to a first-order $n = 4$ transition (Fig. 23). The β exponent associated with a Lifshitz point is expected to be about 0.25 as described above.

BaMnF₄ has been shown to exhibit a soft-mode behavior similar to several other structural phase transitions,⁴⁵ that is, a soft mode which is overdamped, but becomes underdamped both as the temperature is increased above T_c and \bar{q} deviates from the soft-mode wave vector, \bar{q}_1 . In addition, there is a

resolution limited central peak which diverges as $T - T_c$ approaches zero. The major difference is that \bar{q}_1 has an incommensurate value whereas most other structural phase transitions have $\bar{q}_1 = 0$ or some other commensurate value.

Below T_c , BaMnF₄ exhibits superlattice peaks at $\bar{q}_1 = (0.39, 0.5, 0.5)$. Other satellites are observed at $\bar{q}_2 = 2\bar{q}_1$ and $\bar{q}_3 = 3\bar{q}_1$ which could be either harmonics of \bar{q}_1 or secondary order parameters. The surprising feature of this incommensurability is that \bar{q}_1 does not vary with temperature and never locks in at any commensurate wave vector. On this basis, the incommensurability could be due to a peculiarity in the low-temperature structure which is insensitive to any fluctuations which would drive it commensurate.

The discussion of the dynamics above suggests that there should be four additional modes of vibration in the low-temperature phase corresponding to two amplitude modes and two phase modes (one of which has zero frequency). We were unable to observe any of these features. This may be due to the large elastic scattering of the satellite peaks and relatively strong paramagnetic scattering from the Mn²⁺ ions which increases as T is lowered toward T_N .

ACKNOWLEDGMENTS

We thank J. F. Scott and G. A. Samara for sending reports of their work prior to publication. We have benefitted from discussions with S. Aubrey, J. D. Axe, A. D. Bruce, and G. Shirane. Research at Brookhaven supported by Division of Basic Energy Sciences, DOE, under Contract No. EY-76-C-02-0016.

*Permanent address: Dept. of Phys., Univ. of Edinburgh, Edinburgh, Scotland.

¹M. Eibschütz and H. J. Guggenheim, *Solid State Commun.* **6**, 737 (1968).

²M. Eibschütz, H. J. Guggenheim, S. H. Wemple, I. Camlibel, and M. DiDomenico, *Phys. Lett. A* **29**, 409 (1969).

³M. DiDomenico, M. Eibschütz, H. J. Guggenheim, and I. Camlibel, *Solid State Commun.* **7**, 1119 (1969).

⁴K. C. Cousseins and M. Samouël, *C. R. Acad. Sci. Ser. C* **265**, 1121 (1967).

⁵E. T. Keve, S. C. Abrahams, and J. L. Bernstein, *J. Chem. Phys.* **51**, 4928 (1969).

⁶H. G. von Schnering and P. Bleckmann, *Naturwissenschaften* **55**, 342 (1968).

⁷J. K. Brandon and H. D. Megaw, *Philos. Mag.* **21**, 189 (1970).

⁸L. Holmes, M. Eibschütz, and H. J. Guggenheim, *Solid State Commun.* **7**, 973 (1969).

⁹B. I. Al'shin, D. N. Astrov, and R. V. Zorin, *Zh. Eksp.*

Teor. Fiz. **63**, 2198 (1972) [*Sov. Phys. JETP* **36**, 1161 (1973).]

¹⁰D. E. Cox, M. Eibschütz, H. J. Guggenheim, and L. Holmes, *J. Appl. Phys.* **41**, 943 (1970).

¹¹M. Eibschütz, L. Holmes, H. J. Guggenheim, and D. E. Cox, *J. Phys.* **32**, C759 (1971).

¹²E. G. Spencer, H. J. Guggenheim, and G. J. Kominiak, *Appl. Phys. Lett.* **17**, 300 (1970).

¹³J. Barak, D. Fekete, N. Kaplan, and H. J. Guggenheim, *J. Magn. Magn. Mater.* **1**, 153 (1975).

¹⁴R. V. Zorin, B. I. Al'shin, D. N. Astrov, and A. V. Tishchenko, *Fiz. Tverd. Tela (Leningrad)* **14**, 3103 (1972) [*Sov. Phys. Solid State* **14**, 2661 (1973).]

¹⁵S. V. Petrov, M. A. Popov, and L. A. Prozorova, *Zh. Eksp. Teor. Fiz.* **62**, 1884 (1972) [*Sov. Phys. JETP* **35**, 981 (1972).]

¹⁶E. L. Venturini and R. P. Morgenthaler, in *Proceedings of the 20th Conference on Magnetism and Magnetic Material, San Francisco, Calif.-1974*, edited by C. D. Graham, Jr., G.

- H. Lander, and J. J. Rhyne, AIP Conf. Proc. No. 24 (AIP, New York, 1975), p. 168.
- ¹⁷D. L. Fox and J. F. Scott, J. Phys. C 10, L329 (1977).
- ¹⁸J. F. Ryan and J. F. Scott, Solid State Commun. 14, 5 (1974).
- ¹⁹Yu. A. Popkov, S. V. Petrov, and A. P. Mokhir, Fiz. Nizk. Temp. 1, 189 (1975) [Sov. J. Low Temp. Phys. 1, 91 (1975).]
- ²⁰I. J. Fritz, Phys. Lett. A 51, 219 (1975); Phys. Rev. Lett. 35, 1511 (1975).
- ²¹D. W. Bechtle and J. F. Scott, J. Phys. C 10, L209 (1977).
- ²²G. A. Samara and P. M. Richards, Phys. Rev. B 14, 5073 (1976).
- ²³A. Levstik, R. Blinc, P. Kadaba, S. Cizikov, I. Levstik, and C. Filipic, Ferroelectrics 14, 703 (1976).
- ²⁴G. A. Samara and J. F. Scott, Solid State Commun. 21, 167 (1977).
- ²⁵V. Dvorak, Phys. Status Solidi B 71, 269 (1975).
- ²⁶A preliminary account of this work has been reported by S. M. Shapiro, R. A. Cowley, D. E. Cox, M. Eibschütz, and H. J. Guggenheim, in *Proceedings of the Conference on Neutron Scattering*, edited by R. M. Moon (NTIS, Springfield, Virginia 22161), p. 399.
- ²⁷H. M. Rietveld, J. Appl. Crystallogr. 2, 65 (1969).
- ²⁸A. W. Hewat, in U. K. Atomic Energy Authority Research Group Report No. RRL-73-897, 1973 (unpublished).
- ²⁹Data in the region of the two satellite peaks described in Sec. II A were excluded from these refinements.
- ³⁰R. E. Watson and A. J. Freeman, Acta Crystallogr. 14, 27 (1961).
- ³¹M. Eibschütz, L. Holmes, H. J. Guggenheim, and D. E. Cox, Phys. Rev. B 6, 2677 (1972).
- ³²R. A. Cowley, G. Shirane, R. J. Birgeneau, and H. J. Guggenheim, Physica (Utrecht) B 86-88, 639 (1977).
- ³³D. E. Moncton, J. D. Axe, and F. J. Di Salvo, Phys. Rev. B 16, 801 (1977).
- ³⁴M. Iizumi, J. D. Axe, G. Shirane, and K. Shimaoka, Phys. Rev. B 15, 4392 (1977).
- ³⁵K. Gesi, J. D. Axe, G. Shirane, and A. Linz, Phys. Rev. B 5, 1933 (1972).
- ³⁶S. M. Shapiro, J. D. Axe, G. Shirane, and T. Riste, Phys. Rev. B 6, 4332 (1972).
- ³⁷O. V. Kovalev, *Irreducible Representations of the Space Groups* (Gordon and Breach, New York, 1965).
- ³⁸D. Mukamel, Phys. Rev. Lett. 34, 481 (1975).
- ³⁹D. Mukamel and S. Krinsky, Phys. Rev. B 13, 5065 (1976); 13, 5078 (1976).
- ⁴⁰K. G. Wilson and J. Kogut, Phys. Rep. C 12, 75 (1974).
- ⁴¹A. D. Bruce and R. A. Cowley, J. Phys. C (to be published).
- ⁴²P. Bak and D. Mukamel, Phys. Rev. B 13, 5086 (1976).
- ⁴³W. L. McMillan, Phys. Rev. B 14, 1496 (1976).
- ⁴⁴R. M. Hornreich, M. Luban, and S. Shtrikman, Phys. Rev. Lett. 35, 1678 (1975).
- ⁴⁵G. Shirane, Rev. Mod. Phys. 46, 437 (1974).